Design and Optimization of Optical Links Based on VHDL-AMS Modeling

Pascal Bontoux, Fabien Mieyeville, Ian O'Connor, Frederic Gaffiot and Gilles Jacquemod
LEOM – UMR 5512 Ecole Centrale de Lyon 69131 Ecully Cedex FRANCE
http://leom.ec-lyon.fr/index.html

Abstract

This paper presents some examples of behavioral model hierarchies for optronic and photonic devices. The methods used to overcome the limitations of VHDL-AMS[1] in modeling propagation phenomena are described. This work is part of an ongoing development of mixed-domain simulation tools for the design of optical links in a standard EDA[2] framework.

1 Introduction

In the near future, interconnects will be a major obstacle to the progression of electronic system performance. According to the ITRS[1], next generation technologies will impose specifications that metallic interconnects will not be able to reach. Optical interconnects may constitute a suitable alternative to overcome these constraints.

Depending on the length of the optical link, different technological solutions have been put forward: board to board or chip to chip interconnects generally use Smart Pixels (based on VCSELs[3] and integrated detectors), while on-chip interconnects are based on integrated photonic devices (microsources, optical waveguides, microresonators, photonic bandgap devices, etc.). The development of these alternative solutions is however viable only if CAD tools exist.

Generally, the trade-off in simulation time against accuracy makes it necessary to build a hierarchy of models: fast, high-level abstraction models are needed to perform the simulation of large systems; and "physics-based" models are necessary to obtain accurate results at the low level. In the case of multi-domain systems, one of the main difficulties is to establish a clear, univocal hierarchy of the different levels of abstraction. This is due to the strong interaction between components arising from non-electronic phenomena (for example, the propagation of the optical field in a guide depends not only on its own parameters, but also on the characteristics of the light source). Thus, because of the diversity of component behavior involved in optronic systems, a unique hierarchy, where each level is associated with a single dedicated simulation engine, is not sufficient. An effective CAD tool should bring together different modeling techniques and simulation algorithms. VHDL-AMS is a language capable of answering these needs [2].

However, in the case of optical devices and systems, the main problem with VHDL-AMS is undoubtedly its inability to translate partial differential equations such as Maxwell's equations, which describe light propagation. This paper shows that it is nevertheless possible to overcome this fundamental limitation.

The first part of this paper deals with the behavioral modeling of smart pixel based links: optronic devices and physical phenomena involved in such a link may be modeled without using propagation equations. VHDL-AMS is thus well suited to carry out transient mixed-domain simulations.

The second part of this paper presents on chip interconnect modeling. In this case, photonic integrated devices require that propagation phenomena should be taken into consideration and VHDL-AMS is used as a common description language for different simulation engines.

2 VCSEL

2.1 Device presentation

VCSELs are a promising generation of optical sources and appear well-suited to photodetection. Low production costs result from the straightforward fabrication of two-dimensional arrays, the possibility for wafer-level testing, and their compatibility with flip-chip bonding techniques. In terms of performance, they provide a single longitudinal mode operation, a small divergence angle and a low threshold current.

[1] Analog and Mixed Signal extension to VHDL, IEEE standard 1076.1
[2] Electronic Design Automation
[3] Vertical Cavity Surface Emitting Lasers

Also, their low power consumption and operating voltage make them compatible with simple drive circuits.

Fig. 1 shows the schematic of a top-emitting index-guided AlGaAs VCSEL processed at LETI (France) [3] which was used for validation.

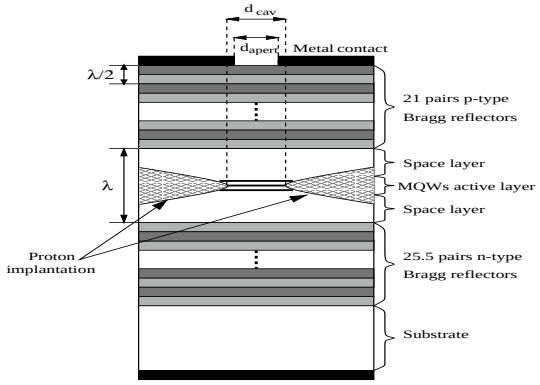

Figure 1: Structure of the VCSEL.

2.2 Rationale for the use of VHDL-AMS

In the implementation of VCSELs in optoelectronic integrated circuits, the thermal and optical interaction with other devices have to be considered, as well as electrical interaction. Also, it is essential to be capable of performing DC, AC and transient simulations of these devices for the design and analysis of any optoelectronic system. For such simulations, a two- or three-dimensional algorithm is not suitable because of the simulation time constraints. One way of overcoming this problem is the implementation of the electrical equivalent circuit in SPICE simulators (macromodeling). Even if such an approach was to be successfully applied to lasers and even to VCSELs, several drawbacks would have to be taken into consideration. First, the modification of any parameter implies that at least a major part of the equivalent circuit needs to be modified. In addition, the resulting relative difficulty of linking the physical behavior to the equivalent circuit elements has to be taken into account. Furthermore, optical component model equations, often describing purely optical phenomena, must be solved numerically, and this separately by an external program which has to be linked to the circuit simulator. And lastly, an equivalent circuit implementation is demanding in terms of simulation time and stability conditions. Consequently, we have adopted another process (behavioral modeling) which enables us, by the implementation of a relatively simple physical model, to improve device performance via feedback to process engineers, while also shortening design cycles.

In the case of this device, all the propagation phenomena can be approximated to a single dimension by averaging all the magnitudes and phenomena on the VCSEL surface. Hence, VHDL-AMS can be used without restriction since all situations necessitating a finite-element type of analysis have been removed.

2.3 The behavioral model

The behavior of a VCSEL is complex and several interactions come into play, as shown in Fig. 2.

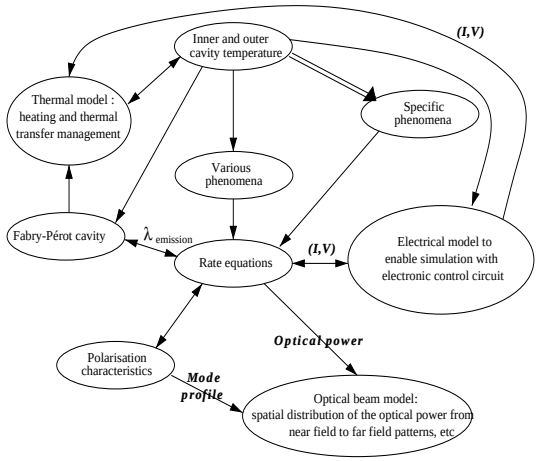

Figure 2: Synopsis of the VCSEL.

Since the numerous interactions cover different domains, it is worth stressing at this point the convenience and relevance of the use of VHDL-AMS.

We are aiming for a temperature dependent, physically based model. The core of the model thus lies in rate equations, used in conjunction with a basic thermal equation and electrical equations. Self-heating in a semiconductor laser has several effects on the performance and cannot be neglected. Rigorous analysis of the thermal behavior of VCSELs requires rather involved numerical calculations [4]. Nevertheless, the following equation (1) [5] provides a basic and convenient approximation which includes heat sources, heat flows and thermal properties of VCSELs:

$$C_{th}\frac{\partial T}{\partial t} = (P_{IV} - P_{optical}) - \frac{\Delta T}{R_{th}} \qquad (1)$$

The well-known single-mode rate equations can be, by extension [5], [6], [7], used to describe the VCSEL's static and dynamic properties. Furthermore, by providing a comprehensive description of physical phenomena inherent to the VCSEL behavior, the rate equations are well suited to a behavioral description.

The rate equations discussed previously can be found in similar forms throughout the literature [8].

They have been modified in order to include temperature:

$$\frac{dN}{dt} = \eta_i \frac{J}{qN_{qw}d_{qw}} - v_{gr}g(N,T,\lambda_{FP})\frac{S}{1+\epsilon S} - R(N) \quad (2)$$

$$\frac{dS}{dt} = \Gamma v_{gr}g(N,T,\lambda_{FP})\frac{S}{1+\epsilon S} - \frac{S}{\tau_p} + \beta N^2 \quad (3)$$

Parameters are adjusted so as to fit the experimental curves. This gain formulation allows us to remain close to physical phenomena and should enable the description of any VCSEL cavity optical gain with sufficient accuracy (in the context of the simulation of optical links).

However, it is important to note the complexity of the system that VHDL-AMS has to solve.

We are aiming at modeling an optical link based on free space propagation and terminating with a quadratic photodetector. Consequently, it is necessary to determine the intensity distribution of the light within the beam in order to complete the model.

The output power of a VCSEL can simply be related to the the photon density [9]. The VCSEL beam is assumed to be Gaussian; the equation that enables the calculation of the optical power received by a photodetector placed at a position z_{ph} from the VCSEL can be found in the literature [10].

2.4 Problems encountered with VHDL-AMS

Two sorts of problem had to be solved and were both due to the simulation engine used (Eldo).

First and foremost, the optical magnitudes are regularly much larger than those typically found in the electronic domain: for example, the carrier density and the photon density are often in excess of 10^{20}, whereas the simulator cannot handle variables with values higher than 10^{12}. This means that when we set these densities to their initial values in the first simulation step, the simulator generates a non-convergence error. Our solution was to scale all the equations so as to keep all variable values below the 10^{12} maximum, while at the same time taking care that the smallest values in the equations remain significantly larger than machine rounding.

The second problem to be resolved was due to the strong non-linearity of the equations. The equations describe the transient as well as the static behavior by setting all time derivatives to zero. Because of the strong non-linearity of the equations, the simulator fails to converge to a DC solution and consequently disrupts any other type of simulation (transient, harmonic) based on the DC solution. Ideally, the formal solution of the system should be generated; however, no commercial mathematical software is presently capable of delivering this solution, essentially due to the logarithmic part of the optical gain expression. A numerical approximation to the DC solution was thus developed in order to make the model convergent. The accuracy of this DC solution (with respect to that which would be generated by established equations) needs to be high when using the solution as starting point for transient and harmonic simulation. If this is not the case, then these analyses fail to converge.

In this case, the DC solution was elaborated by a minor simplification of the established equation, which enabled very good matching between the real and approximated DC solutions.

2.5 Steady-State characteristics of VCSELs

Fig. 3 shows the measured light-current characteristics (source: LETI, France) with different cavity and dielectric aperture ratios. The simulation results are also plotted in this figure.

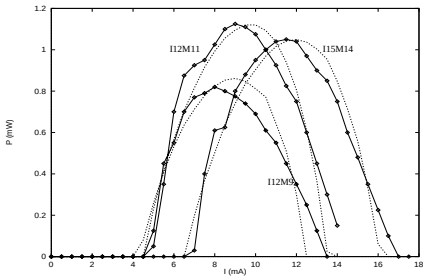

Figure 3: Comparison of experimental and simulated (dashed curves) light-current characteristics of VCSELs with different cavity and aperture diameters.

The simulation results fit the experimental curves with a maximum error of 10%: the results concerning the threshold current match with a maximum error of 5%.

2.6 Transient and harmonic analysis results

The stability and precision of the DC analysis descibed above allows the possibility of running convergent transient and harmonic analysis.

We have simulated (fig. 4), on a Sun Sparc 5 workstation, a pre-biased 450Mb/s data emission: the simulation time is about 5 minutes. The optical output power results are quite similar to those found in the literature. Transient results have not been validated experimentally, but they can be supposed sufficiently viable since based on both a true validated DC analysis and recognized rate equations.

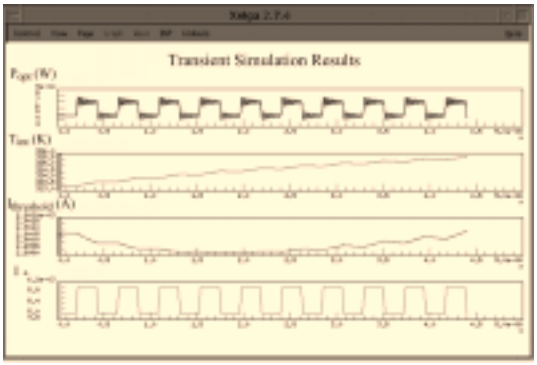

Figure 4: Transient analysis results of optical output power, inner cavity temperature, threshold current variation and input current

It is important to note that the inner-cavity temperature and threshold conditions require a few periods to stabilize to a constant value. Future work can exploit this property to develop a simplified thermal model for transient analysis. This can subsequently be used in a higher-level model to simulate data emission with reduced simulation time.

The AC behavior has not yet been validated experimentally. Nevertheless, the bandwidth values resulting from simulation match those found in the literature.

2.7 Conclusions

Our VCSEL behavioral model is physics-based and includes all major loss mechanisms that can potentially limit the device performance. It is quite generic, convergent in all type of analysis and gives rise to simulation times which are compliant with system design cycles. We can conclude that although VHDL-AMS is not aimed primarily at the simulation of optoelectronic devices, it can still fit depending on the device considered. Reservations have to be expressed concerning devices where finite-element type analysis cannot be circumvented.

3 On-chip Interconnect

As in telecommunication applications, optical interconnects may also be used in photonic or hybrid integrated circuits. However, their use is conditional on the availability of optical device libraries compatible with standard IC design flows. To address this need, we consider VHDL-AMS as capable of building a self-consistent model hierarchy (with or without the aid of a backplane finite-element simulator). However, numerical techniques are also required to simulate an optronic or optical component at the device-level; this approach targets post-layout simulation.

In this section, we examine the possibility of modeling integrated optics and present the necessary link between VHDL-AMS and a FEMs simulator to achieve a complete design flow.

3.1 Straight waveguide and coupled parallel waveguides

We can describe propagation in a waveguide by equation (4):

$$\tan hd = \frac{2hp}{p^2 - h^2} \tag{4}$$

where $p = \sqrt{n_1^2 k^2 - \beta^2}$, $h = \sqrt{\beta^2 - n_2^2 k^2}$ and $k = \frac{2\pi}{\lambda}$. n_1 and n_2 respectively represent the material and the air refractive index, λ is the free wavelength. β is the propagation constant, the crux of the equation.

Equation (4) does not converge with the VHDL-AMS simulation engine, so we have rewritten it in the following form

$$\frac{hd}{2} = \frac{kd}{2}\sqrt{n_1^2 - n_2^2} \cdot \cos\frac{hd}{2} \tag{5}$$

Parallel waveguides exhibit (fig. 5) coupling phenomena, dependent on the modal propagation constant β, physical and geometrical parameters.

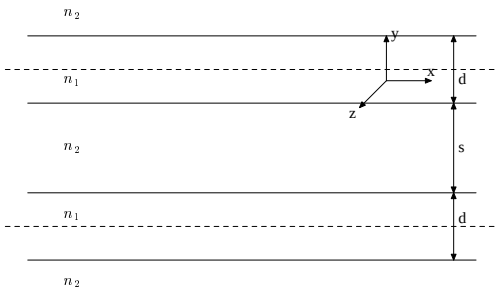

Figure 5: Geometry of two parallel waveguides

Equation (6) describes the coupling constant g:

$$g = \frac{2p^2 h \exp(-hs)}{\beta\left(d + \frac{2}{h}\right)(h^2 + p^2)} \tag{6}$$

where s represents the distance between the two parallel waveguides. The distance at which a complete power transfer occurs from one waveguide to another is given by $L_{\text{trans}} = \frac{\pi}{2g}$[11].

We will now describe the implementation of the modal constant propagation model in VHDL-AMS. This is possible since the above equations are algebraic.

Fig. 6 shows the results of a transient simulation (with Eldo) of the VHDL-AMS coupling model previously described. The simulation gives the output

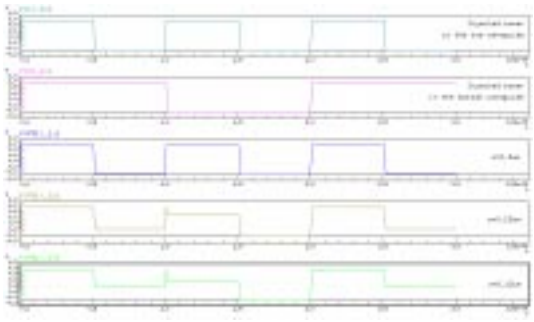

Figure 6: Upper straight waveguide output

power of the top waveguide for various distances between the waveguides (0.3μm, 0.2μm, 0.15μm).

This simulation requires less than one second to be achieved on a Sparc5 workstation.

3.2 Microring resonators

Microring resonators [12] can be used as a basic component in order to build an integrated interconnect network based on wavelength routing. A simple ring resonator evanescently side coupled to a pair of signal waveguides is depicted in figure 7.

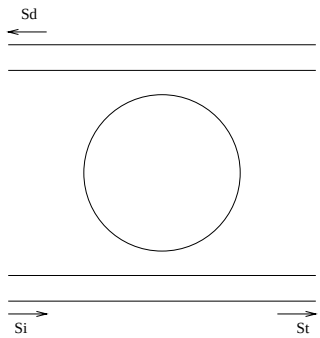

Figure 7: Microring resonator filter

As described in [12], we have the following power transfer characteristics by considering a steady state incident signal S_i with time dependency $S_i \propto \exp[j\omega t]$.

$$S_t = \frac{j(\omega-\omega_0)+\frac{1}{\tau}-\frac{2}{\tau_e}}{j(\omega-\omega_0)+\frac{1}{\tau}}\cdot S_i \quad (7a)$$

$$S_d = \frac{\frac{2}{\tau_e}}{j(\omega-\omega_0)+\frac{1}{\tau}}\cdot S_i \quad (7b)$$

where $\frac{1}{\tau}=\frac{2}{\tau_e}+\frac{1}{\tau_l}$. τ_e and τ_l are the decay rates related, respectively, to the power leaving the input waveguide/ring and the power lost by surface scattering. ω and ω_0 represent, respectively, the input frequency and the resonant frequency.

3.2.1 Computation of resonant frequencies

Firstly, we must determine the resonant frequencies ω_0 of the filter. The implicit equation which gives us the resonant frequencies in terms of the azimuthal mode number and the radius mode number can be found in [13]. Unfortunately, we cannot compute the resonant wavelength with the Eldo simulation engine for two reasons: firstly, we must give an operating point sufficently close to the solution, but we do not know *a priori* even an approximate value; and secondly, we need to know all the solutions in a given range wavelength, but we do not know the number of the solutions.

To overcome this problem, we have implemented an algorithm in C which solves the previous equation and passes the different resonant frequency values to the microring model.

3.2.2 Coupling parameter computation

To simplify the model, we neglect the loss due to intrinsic effects, so $\frac{1}{\tau}\simeq\frac{2}{\tau_e}$. We find from [12] a link between τ_e and κ^2 which represents the fraction of power coupled out of the ring over the interaction region.

The expression for κ is given in [14]. This coefficient is dependent on the geometrical and physical parameters and the transverse propagation constant in the core. This latter constant depends on the same coefficients but it is given by an implicit equation such as equation (5). Thus, the implementation and the computation of the coefficient is possible via the Newton-Raphson algorithm in VHDL-AMS.

3.2.3 Transfer function expression

From the formulation of S_d, we can obtain a power transfer function in the frequency (eq. (8)) and time (eq. (9)) domains:

$$H(\omega)=\frac{S_d^2}{S_i^2}=\frac{\frac{4}{\tau^2}}{\frac{4}{\tau^2}+(\omega-\omega_0)^2} \quad (8)$$

$$h(t)=\frac{4\exp(i\omega_0 t)}{\tau}\cdot\exp\left(-\frac{2}{\tau}|t|\right) \quad (9)$$

with $P_s(t)=h(t)\otimes P_e(t)$, $P_x(t)=[S_x(t)]^2$.

In order to solve this equation, the absolute value of the infinite-impulse response (IIR) $h(t)$ is approximated by a 1$^{\text{st}}$ order recursive numerical filter and thus computes the convolution numerically:

$$P_s(kT_e)=\frac{4}{\tau}\cdot P_e(kT_e)+a\cdot P_s((k-1)T_e) \quad (10)$$

where $a = \exp\left(-\frac{2T_e}{\tau}\right)$ and T_e is the sampling period. Finally, we can compute step by step the output power value.

3.3 FEMs requirement

Different levels of abstraction are not always supported by electrical simulators, particularly at the device level and also at the layout level. In the case of integrated optical device simulation, computational electromagnetics methods are required.

In cases where the optical carrier cannot be neglected, the use of a method which solves Maxwell's equations is necessary. The Finite-Difference Time-Domain (FDTD) algorithm [15] is one of the most popular numerical methods for the solution of problems in electromagnetics. The FDTD algorithm is based on a second-order approximation to Maxwell's equations accurate in both time and space. Accuracy can be kept high and numerical dispersion small by having a sufficient number of grid spaces per wavelength. Its main disadvantage is that it is expensive in terms of memory and CPU time.

In order to simulate systems containing both electronic and optical devices, a link between VHDL-AMS and a Finite-Elements method is required. Two main approaches exist: the first consists of considering 3 simulators: analog, digital and FEM, interconnected by a co-simulation bus. The second focuses on a Spice-like simulator as a single simulation engine and a simulator based on a FDTD algorithm encapsulated in a VHDL-AMS architecture. The latter is more interesting, because of the system level designer does not know that the FDTD algorithm was used. Unfortunately, the FDTD algorithm was called for each computational step of the electrical simulator and the time necessary for simulation was not acceptable for system level simulation.

4 Summary and Conclusions

We have shown that optoelectronic devices such as VCSELs and passive components for optical interconnects can be modeled using the VHDL-AMS standard language. Some limitations of the language may be pointed out. The lack of specific structures able to handle high frequency phenomena penalizes accuracy and computation speed for system level simulation. From the device designer's point of view, the language should provide a direct interface to a partial differential equations solver. Thus, to take into account the particular characteristics of these problems, future developments of HDL's should provide links to different simulation engines. Nevertheless, this work shows that it is possible to simulate complex systems, including optics, with VHDL-AMS.

References

[1] Semiconductor Industry Association, "International technology roadmap for semiconductors technology," 1998.

[2] F. Gaffiot *et al.*, "Behavioral modeling for hierarchical simulation of optronic systems," *IEEE Trans. Circuits and Systems II*, vol. 46, no. 10, Oct. 1999.

[3] Laurent Georjon, *Conception et caractérisation de lasers à cavité verticale*, Ph.D. thesis, Commissariat à l'Energie Atomique – Laboratoire d'Electronique de Technologie et d'Instrumentation, Oct. 1997.

[4] W. Nakwaski *et al.*, "Thermal properties of vertical-cavity surface-emitting semiconductor lasers," in *Progress in Optics XXXVIII*, chapter III, pp. 165–262. North Holland, 1998.

[5] S.F. Yu *et al.*, "Theoretical analysis of modulation response and second-order harmonic distortion in vertical-cavity surface-emitting lasers," *IEEE J. Quantum Electron.*, vol. 32, no. 12, pp. 2139–2147, Dec. 1996.

[6] Brent K. Whitlock, *iFROST : a CAD for modeling and simulation of optical interconnects*, Ph.D. thesis, University of Illinois at Urbana-Champaign, 1996.

[7] J.J. Morikuni *et al.*, "Spatially independent VCSEL models for the simulation of diffusive turn-off transients," *J. Lightwave Technol.*, vol. 17, no. 1, pp. 95–102, Jan. 1999.

[8] S.F. Yu, "Dynamic behavior of vertical-cavity surface-emitting lasers," *IEEE J. Quantum Electron.*, vol. 32, no. 7, pp. 1168–1179, July 1999.

[9] S.A. Javro *et al.*, "Transforming Tucker's linearized laser rate equations to a form that has a single solution regime," *J. Lightwave Technol.*, vol. 13, no. 9, pp. 1899–1904, Sept. 1995.

[10] Y.-G. Zhao *et al.*, "Far-field and beam characteristics of vertical-cavity surface-emitting lasers," *Appl. Phys. Lett.*, vol. 69, no. 13, pp. 1829–1831, Sept. 1996.

[11] Amnon Yariv, *Optical Electronics in Modern Communications*, Oxford University Press, fifth edition, 1997.

[12] B. E. Little *et al.*, "Microring resonator channel dropping filters," *J. Lightwave Technol.*, vol. 15, no. 6, June 1997.

[13] R. P. Wang *et al.*, "Theory of optical modes in semiconductor microdisk lasers," *J. Appl. Phys.*, vol. 81, no. 8, Apr. 1997.

[14] H. A. Haus *et al.*, "Coupled-mode theory of optical waveguides," *J. Lightwave Technol.*, vol. LT-5, no. 1, Jan. 1987.

[15] Allen Taflove, *Computational electrodynamics - The Finite-Difference Time-Domain Method*, Artech House, 1995.